PHYSICAL REVIEW B VOLUME 24, NUMBER 2 15 JULY 1981

Electron drift velocity and diffusivity in germanium

C. Jacoboni, F. Nava, C. Canali, and G. Ottaviani
Gruppo Nazionale di Struttura della Materia,
Istituto di Fisica, Università di Modena, 41100 Modena, Italy
(Received 5 September 1979)

Experimental results for electron drift velocity and diffusivity in germanium, obtained with the time-of-flight technique in hyperpure material, are presented for temperatures between 8 and 240 K and fields between 1 and 10^4 V/cm oriented along ⟨111⟩ and ⟨100⟩ directions. An anisotropy of the drift velocity and of the diffusion coefficient is found with the electric field applied along ⟨111⟩ and ⟨100⟩ directions, the latter due to the intervalley diffusion. The effect of the electron-electron interaction in the anisotropy properties has also been investigated. Theoretical Monte Carlo calculations have been performed with a model which includes lower, ⟨111⟩, nonparabolic bands as well as upper bands at the center of the Brillouin zone and along the ⟨100⟩ directions. Acoustic scattering with proper energy relaxation, optical scattering, and intervalley scattering between equivalent and nonequivalent valleys has been taken into account. Besides drift velocities and diffusion coefficients, other quantities such as mean electron energy, electron distribution function, and valley repopulation have been obtained from the Monte Carlo simulation.

I. INTRODUCTION

This is the fourth paper of a series of four which present experimental and theoretical investigations on transport properties of charge carriers in silicon and germanium.[1–3] The purpose of this paper is to describe a detailed analysis of drift velocity and diffusivity of electrons in germanium. Like the three previous papers, this investigation is intended to be as extensive and detailed as is possible at the present time.

On the experimental side, we have used the purest available crystals and the time-of-flight technique, which is one of the most reliable experimental techniques for high-resistivity materials. We tried to extend as much as possible the range of temperatures and field strength investigated.

On the theoretical side, we have used the Monte Carlo technique with a physical model which includes most of the known features of the band structure and the scattering mechanisms of electrons in germanium. In particular, besides the lowest ⟨111⟩ valleys, the upper valleys, at the Γ point and along the ⟨100⟩ directions have been included, as well as nonparabolicity of the lowest valleys. It was thus possible to estimate how much nonparabolicity and upper valleys contribute, in the present model, to the negative differential mobility (NDM) of electrons at low temperatures and high fields. The relative importance of these two causes is one of the points which have aroused most interest in the literature.[4,5] The effect of electron-electron interaction on the valley repopulation is also analyzed.

Finally, the diffusion of electrons along the direction of the field is investigated both experimentally and theoretically. An anisotropy of the diffusion coefficient is found with the electric field, $\vec{E}$, applied along ⟨111⟩ and ⟨100⟩ directions which is due to intervalley diffusion.

Section II contains a description of the experimental results with only a few comments on the experimental technique, already described in previous papers,[1–3,6,7] and on the samples used. In Sec. III the theoretical model and the Monte Carlo technique are described. Section IV contains a comparison and a discussion of experimental and theoretical results; in this section all ancillary results obtained by Monte Carlo simulation (as mean energies, energy relaxation times, valley repopulations, electron distribution functions, and relative efficiencies of the different scattering mechanisms) are shown to give a complete picture of the transport process. Some conclusive remarks are presented in Sec. V. The Appendix contains mathematical details of the treatment of acoustic scattering in nonparabolic bands used in the Monte Carlo program.

In order to give a unitary and complete picture of electron transport properties in germanium, some results previously disclosed in short publications,[8,9] have been included in the present paper.

II. EXPERIMENTAL TECHNIQUE AND RESULTS

A. Time-of-flight technique and samples

The time-of-flight technique[1–3,6,7] is based on the analysis of the current pulse due to charge carriers

created by a suitable ionizing radiation and traveling, under the influence of an applied electric field, across a sample of known thickness W. Since this topic has been treated in several papers, we recall here only its principal features.

In the experiment a sheet of electron-hole pairs is created near the negative contact of the sample by a short burst ($\approx$70–100 ps) of 25-keV electrons whose range R is much shorter ($\leq$2.5 μm) than the sample thickness. The pair density can be changed by changing the current of the primary electrons. Electrons and holes are separated by the applied electric field, and the electrons drift across the sample toward the opposite contact. This propagation of the electron charge layer gives rise to a transient current which is used to measure the transit time T_R and to obtain the drift velocity $v_d = W/T_R$. The broadening of the electron layer crossing the sample due to the longitudinal diffusion, produces a fall time τ_F of the current pulse longer than the rise time τ_R. The longitudinal diffusion coefficient can be obtained by means of the equation[7]

$$D_l = \frac{(\tau_F^2 - \tau_R^2) v_d^3}{21.6\, W} , \qquad (1)$$

where τ_F and τ_R are defined between 0.05 and 0.95 of the pulse height. The advantages of the time-of-flight technique for measuring v_d and D_l for high-resistivity high-purity semiconductors in wide ranges of electric fields and temperatures, and the validity of Eq. (1) have been discussed in several papers.[7,8,10–12]

The samples used in these experiments were n^+-i-p^+ diodes made of high-purity germanium supplied by General Electric and Lawrence Berkeley Laboratory. The n^+ and p^+ contacts were formed by solid-phase epitaxy at 350 °C, using Al and Sb, respectively.[13] The low temperature involved in such a process prevents contamination of the material. Several samples were obtained from the same ingot, cut perpendicular to the crystallographic axes ⟨111⟩ and ⟨100⟩ with an accuracy of ±1°. The sample thicknesses varied from 220 to 790 μm and had a useful area of about 10 mm^2 approximately at the center of 1-cm^2 disks. Their characteristics are reported in Table I of Ref. 3.

A detailed analysis of the experimental errors has been reported in Refs. 1–3, 8, 11, and 12. In the present measurements the total experimental error is estimated to be around ±5% for v_d and ±20% for D_l. The error in evaluating the temperature, measured with a germanium resistor in the range 8–77 K and with a thermocouple in the range 77–220 K, was 0.3 K in the former case and 1 K in the latter. The same drift velocities and diffusion coefficients have been obtained, within the experimental errors, in samples of different thicknesses over the whole range of temperatures and fields examined, supporting the view that the transit time is much longer than the time necessary for the electrons to reach a steady-state condition.[1,12]

B. Drift velocity

In Figs. 1–4 the electron drift velocity is reported as a function of temperature ranging from 8 to 240 K and of electric field ranging from 2 to 10 000 V/cm and applied parallel to the ⟨111⟩ and ⟨100⟩ crystallographic axes. The investigation was not extended to higher temperatures because of problems related to the signal-to-noise ratio. For comparison the experimental results of Smith[14] at 300 K are also reported in Fig. 4. Closed and open symbols refer to experi-

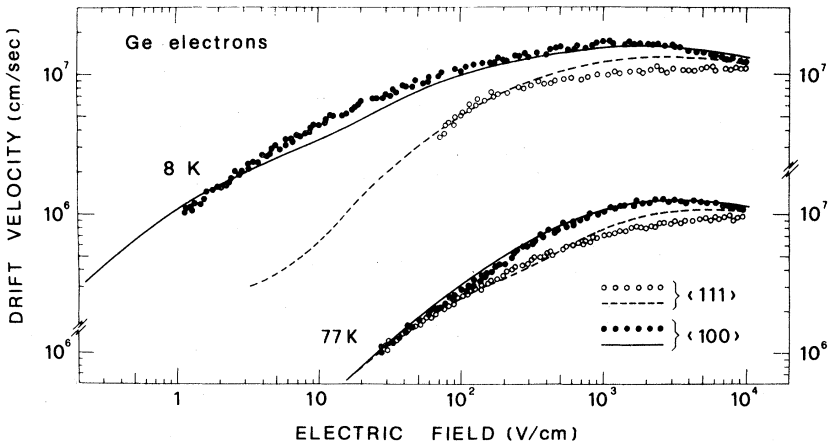

FIG. 1. Electron drift velocity as a function of electric field applied parallel to ⟨100⟩ and ⟨111⟩ crystallographic directions at 8 and 77 K. Closed and open circles refer to experimental data and continuous and broken lines indicate the theoretical results.

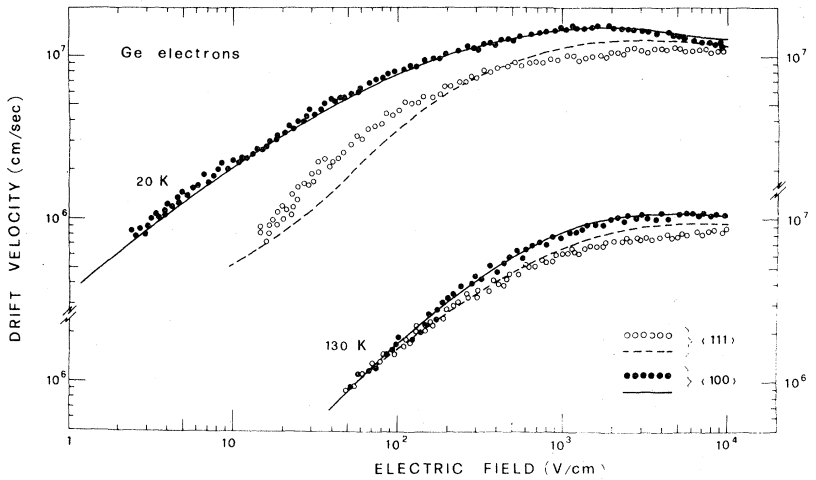

FIG. 2. Electron drift velocity as a function of electric field applied parallel to ⟨100⟩ and ⟨111⟩ crystallographic directions at 20 and 130 K. Closed and open circles refer to experimental data and continuous and broken lines indicate the theoretical results.

mental data obtained with the field parallel to ⟨100⟩ and ⟨111⟩ directions, respectively.

The main features of the experimental results are:

(i) The anisotropy effect increases on decreasing temperatures. The curves of the drift velocities along the two directions ⟨111⟩ and ⟨100⟩ tend to join together at the highest electric field even though such a rejoining was not achieved at all temperatures considered.

(ii) An NDM region was found with $\vec{E} \parallel \langle 100 \rangle$ for temperatures below 130 K at high electric fields. The effect is enhanced by decreasing the temperature. The threshold field, defined as the field at which the drift velocity has the maximum value before the region of NDM, decreases on decreasing temperatures.

(iii) At the highest electric fields applied parallel to a ⟨111⟩ direction a region of drift velocity nearly independent of the electric field is obtained.

(iv) For $T \gtrsim 45$ K the Ohmic region is reached and, as we shall see below, the results are in good agreement with values for the mobility given in the literature. For $T < 45$ K, even at the lowest electric field applied, the drift velocity is not proportional to the electric field indicating that Ohmic condition is

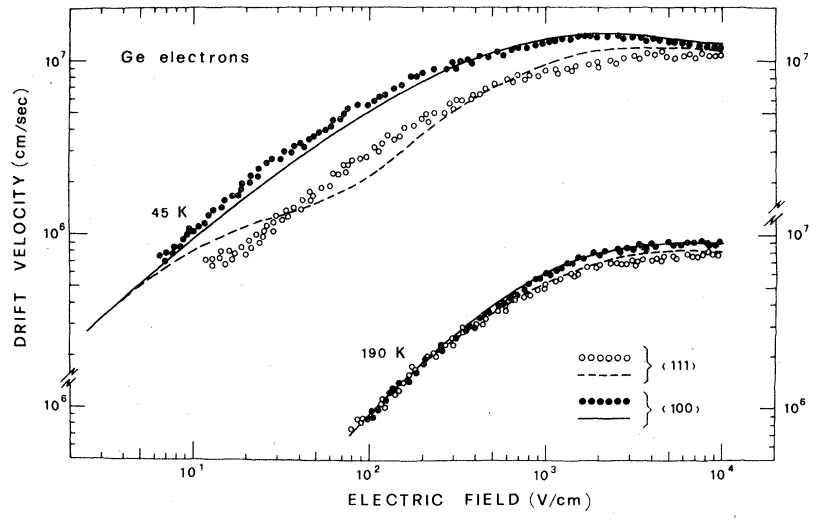

FIG. 3. Electron drift velocity as function of electric field applied parallel to ⟨100⟩ and ⟨111⟩ crystallographic directions at 45 and 190 K. Closed and open circles refer to experimental data and continuous and broken lines indicate theoretical results.

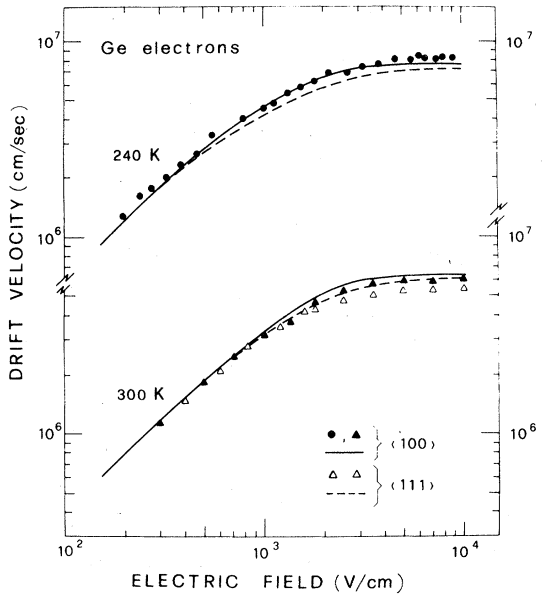

FIG. 4. Electron drift velocity as a function of electric field applied parallel to ⟨100⟩ and ⟨111⟩ crystallographic directions at 240 and 300 K. Continuous and broken lines refer to theoretical calculations; closed circles report present experimental results; open and closed triangles indicate experimental results of Ref. 14.

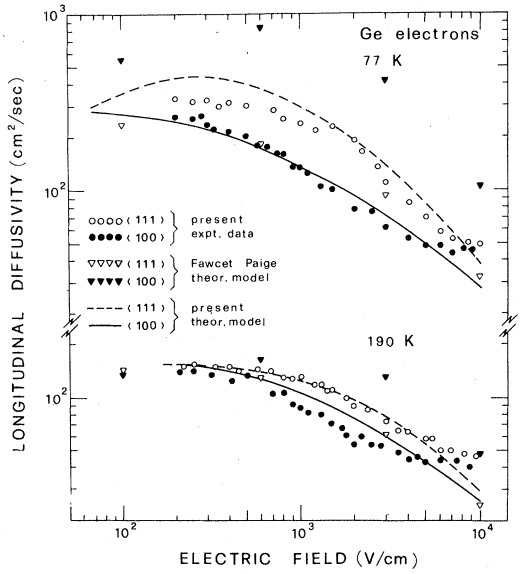

FIG. 5. Longitudinal diffusion coefficients of electrons in germanium as a function of electric field applied parallel to ⟨111⟩ and ⟨100⟩ crystallographic directions at 77 and 190 K. Closed and open circles indicate present experimental data; continuous and broken lines refer to present theoretical results; open and closed triangles report theoretical data obtained with the parameters used by Fawcett and Paige in Ref. 4.

not attained.

(v) For temperatures lower than 77 K and fields parallel to ⟨111⟩ directions, the experimental drift velocities were found to depend on the intensity of the ionizing radiation, that is on the carrier concentration in the electron layer crossing the sample. This effect, due to electron-electron, (e-e), interaction, will be discussed below. For this reason, only the experimental data obtained with the lowest possible carrier concentration have been reported in Figs. 1–4 for ⟨111⟩ directions. In these conditions, however, a severe signal-to-noise problem is encountered, especially at low fields, so that experimental results are interrupted toward lower field strengths.

C. Diffusion coefficients

Figure 5 shows the experimental results for the longitudinal diffusion coefficient of electrons as a function of electric field oriented along ⟨111⟩ and ⟨100⟩ direction at two temperatures. We may note that $D_l(\vec{E})$ decreases with increasing field strength and tends to saturate at fields higher than about 6 kV/cm. This result is similar to that found in Si at 300 K.[15] Furthermore, a very strong anisotropy effect is seen in the longitudinal diffusion with $D_{l\langle 111\rangle} \geqslant D_{l\langle 100\rangle}$. This anisotropy is opposite to the anisotropy of the electron drift velocity, $v_{d\langle 100\rangle} \geqslant v_{d\langle 111\rangle}$. At the highest applied electric fields the experimental results of the diffusion coefficient along the two directions tend to coincide. At the lowest applied field both D_l's tend to the Ohmic value D_0 given by Einstein relation.

D. Electron-electron interaction

In many-valley semiconductors the valley repopulation depends on carrier concentration because e-e interaction tends to equalize the mean energy of electrons in hot and cold valleys. Then the difference of the drift velocity v_d at different field orientations, due to valley repopulation, tends to decrease as e-e becomes more effective. This effect has been observed in Si.[16–18] In standard current-measuring techniques, the carrier concentration is changed by changing the doping, and therefore the impurity concentration also changes; this fact may complicate the interpretation of the phenomenon. With the time-of-flight technique, on the other hand, the concentrations of electrons traveling across the sample can be changed, without changing the impurity content, by changing the intensity of the ionizing beam. In doing so, on increasing electron concentration we saw a decrease of the drift-velocity anisotropy due to an increase of $v_{d\langle 111\rangle}$ for temperatures below 77 K, while the $v_{d\langle 100\rangle}$ values remained practically the same at all

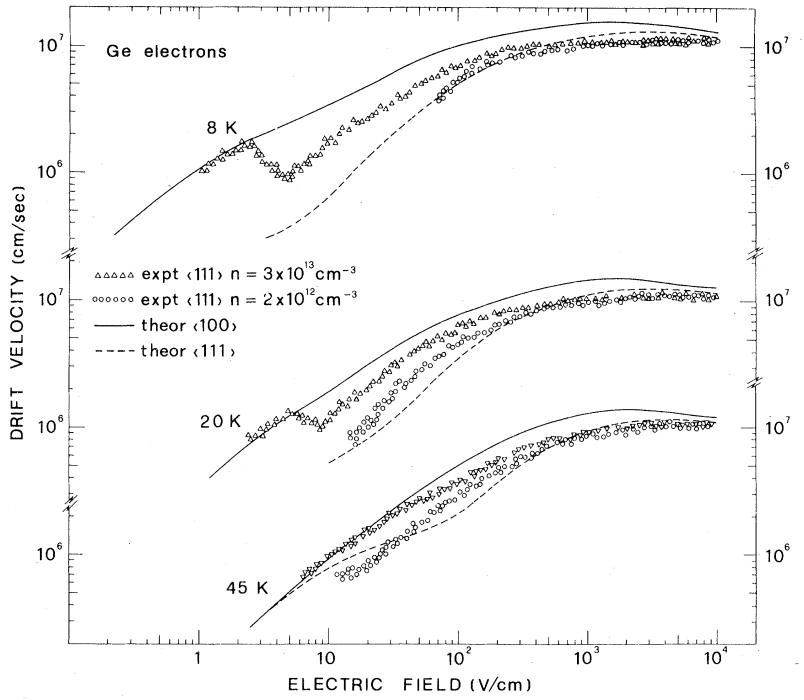

FIG. 6. Electron drift velocity as a function of electric field applied parallel to ⟨100⟩ and ⟨111⟩ crystallographic directions at 8, 20, and 45 K for two different concentrations of the electrons traveling across the sample. Continuous and broken lines indicate the theoretical results reported in Figs. 1–3, without e-e interaction. Circles and triangles refer to experimental results of electron drift velocity for $\vec{E}$ applied parallel to ⟨111⟩ crystallographic direction and two concentrations of electrons created by the electron beam $n = 2 \times 10^{12}$ cm^{-3} and $n = 3 \times 10^{13}$ cm^{-3}, respectively. The experimental data of $v_{d\langle 100\rangle}$ remain the same within the experimental error on changing the electron density.

electron densities. In Fig. 6 experimental results of $v_{d\langle 111\rangle}$ as a function of E at three temperatures are shown. Circles refer to a concentration of created carriers equal to 2×10^{12} cm^{-3}, triangles to a concentration of 3×10^{13} cm^{-3}.

III. THEORY—MONTE CARLO CALCULATIONS

In what follows we shall describe the theoretical model and the Monte Carlo program used to interpret the experimental results. They are essentially of the type described by Fawcett and Paige[4] with the addition of nonparabolicity of the lower valleys, energy dissipation through acoustic scattering, and the correct acoustic-phonon population.

A. Band structure

The absolute minima of the conduction band in germanium lie along the ⟨111⟩ directions at the edge of the Brillouin zone (L points). There are therefore four equivalent such valleys. Taking into account nonparabolicity, the energy $\epsilon^{(i)}$ of an electron in the ith valley is related to $\vec{k}$ by

$$\gamma^{(i)}(\vec{k}) \equiv \frac{\hbar^2}{2}\left[\frac{(k-k_0^{(i)})_l^2}{m_l} + \frac{(k-k_0^{(i)})_t^2}{m_t}\right] = \epsilon^{(i)}(\vec{k})[1+\alpha\epsilon^{(i)}(\vec{k})] \ , \quad (2)$$

where $\vec{k}_0^{(i)}$ indicates the position in the Brillouin zone of the center of the ith valley; α is the nonparabolicity parameters; the subscripts l and t indicate longitudinal and transverse components with respect to the symmetry axis of the valleys; m_l and m_t are the effective masses; the origin of energy has been taken at the minimum of the conduction band.

Upper minima at the center of the Brillouin zone and along the ⟨100⟩ directions have been included in the present model since at high fields electrons populate these valleys also. The central valley has been assumed to be spherical and parabolic; the valleys along the ⟨100⟩ directions have been taken to be parabolic with ellipsoidal shapes. The Herring and Vogt transformation[19] has been applied to the lower ⟨111⟩ and to the upper ⟨100⟩ valleys, to reduce the problem to spherical symmetry.

TABLE I. Set of the physical parameters used in the present calculations to fit experimental results. Phonon symbols in parentheses are used for identification in Fig. 15.

Valleys	Effective mass ratio	Phonon mode or equivalent temperature	Coupling constant
111 (*Ac*)	$m_l = 1.588$ $m_t = 0.081\,52$	Acoustic	11 eV
100	$m_l = 1.353$ $m_t = 0.288$	Acoustic	9 eV
000	$m = 0.037$	Acoustic	5 eV
111 (*OP*)		430 K	5.5×10^8 eV cm^{-1}
111 − $\bar{1}$11 (*IE*1)		320 K	3.0×10^8 eV cm^{-1}
111 − $\bar{1}$11 (*IE*2)		120 K	2.0×10^7 eV cm^{-1}
111 − 100 (*I*15)		320 K	4.06×10^8 eV cm^{-1}
111 − 000 (*I*1*G*)		320 K	2.0×10^8 eV cm^{-1}
100 − $\bar{1}$00		100 K	7.89×10^7 eV cm^{-1}
100 − $\bar{1}$00		430 K	9.46×10^8 eV cm^{-1}
100 − 000		320 K	1.00×10^9 eV cm^{-1}

$\rho = 5.32$ g cm^{-1}; $v_s = 5.4 \times 10^5$ cm s^{-1}; $\alpha = 0.3$ eV^{-1}; $\epsilon_{100} = 0.18$ eV; $\epsilon_{000} = 0.14$ eV.

B. Scattering mechanisms

The electron-phonon scattering mechanisms which have been included in Monte Carlo program are[4] (i)−(iii) acoustic intravalley in all valleys, (iv) optical intravalley in ⟨111⟩ valleys, (v)−(vi) two intervalley between ⟨111⟩ valleys, (vii) one intervalley between ⟨111⟩ and ⟨100⟩ valleys, (viii) one intervalley between ⟨111⟩ and ⟨000⟩ valleys, (ix) one intervalley between ⟨100⟩ valleys, (x)−(xi) two *g* intervalley between ⟨100⟩ valleys, and (xii) one intervalley between ⟨100⟩ and ⟨000⟩ valleys.

Optical and intervalley phonon scattering have been treated with standard procedures.[4,20] The details of the procedure used for acoustic scattering in the nonparabolic valleys including energy relaxation are given in the Appendix.

Scattering from impurities has been neglected owing to the high purity of the material used in the experiments. Electron-electron scattering has been considered in a special Monte Carlo program which will be briefly discussed in a following section.

C. Monte Carlo program and physical parameters

The Monte Carlo program, of the type described in several papers,[4,20–22] includes all 11 valleys explicitly. The equivalence of the valleys equally oriented with respect to the applied electric field has been checked *a posteriori* in the results. Rees self-scattering has been used with a step-shaped total scattering rate[23] in the lowest valleys and a constant total scattering rate in the upper valleys. Four electrons have been simulated at the same time, with their initial $\vec{k}$ situated in the four lowest valleys in order to cover the low-field region at low temperatures when intervalley scattering is essentially absent.[1] The simulation of each electron has been split into many parts of equal time duration to obtain the diffusion coefficient and the statistical uncertainty in the drift velocity as described in Refs. 21 and 23.

In Table I the physical parameters used in the calculations are listed. As can be seen, most of the parameters coincide with the values of set *b* of Fawcett and Paige.[4] Some of them have been slightly changed in order to obtain a better fit of the overall experimental data. In particular the warm electron region at low temperatures and the diffusion coefficients are much better interpreted with the set of constants given here, as will be discussed in the next section. The nonparabolicity parameter for the transverse mass is approximately given by $(2\Delta)^{-1}$, where 2Δ is the energy difference between $\epsilon(L_{1c})$ and $\epsilon(L_{3v})$.[24] Values for 2Δ in the literature[25,26] range from 2.0 to 2.5 eV. Since however the longitudinal direction is much more parabolic, an average value of $\alpha = 0.3$ eV^{-1} has been assumed in the present work.

IV. DISCUSSION OF RESULTS

In Figs. 1–7 a comparison is given between experimental and theoretical results.

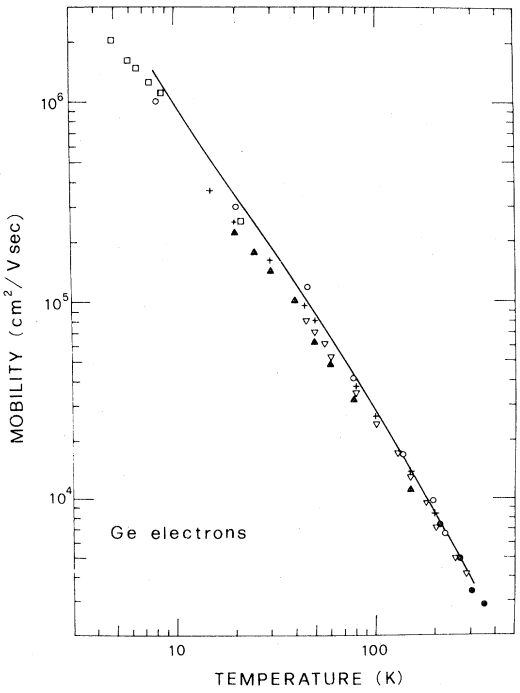

FIG. 7. Ohmic mobility of electrons in germanium as a function of temperature. Open circles indicate our experimental mobilities at the lowest applied fields, which are perfectly Ohmic only for $T \geq 45$ K. The other experimental points refer to data from the literature: closed triangles from Ref. 31, open triangles from Ref. 27, crosses from Ref. 28, closed circles from Ref. 29, and open squares from Ref. 30. The continuous line indicates present theoretical results.

A. Ohmic mobility

Figure 7 represents the electron mobility as a function of temperature. The present experimental values of v_d/E obtained for each temperature at the lowest applied field are reported together with mobility results available in the literature.[27–31] From the analysis of our v_d vs E curves we may conclude that at temperatures above about 45 K the Ohmic region is attained. The continuous line indicates the results of the Monte Carlo simulation. Taking into account the experimental uncertainty and some possible influence of impurity scattering, the agreement between the different sets of experimental data and the theoretical curve is good.

B. Drift velocity

Figures 1–4 show a comparison between experimental and theoretical drift velocities as a function of temperature and electric field. Closed and open symbols represent the experimental data for applied fields oriented along ⟨100⟩ and ⟨111⟩ direction, respectively. Continuous and dashed lines indicate the theoretical results for the same directions. The overall agreement between theory and experiments is satisfactory.

At lower temperatures ($T \lesssim 130$ K) and high fields a negative differential mobility (NDM) is present for $\vec{E}$ applied along a ⟨100⟩ direction. This effect has been found in the past[32–36] and different theoretical interpretations have been published in the literature. Dumke[5] showed that the effect could be due to the presence of band nonparabolicity without invoking upper valleys, while the Monte Carlo calculation of Fawcett and Paige,[4] which used parabolic valleys, attributed the effect purely to the presence of the upper valleys. In their model the NDM phenomenon is attributed to a transfer electron mechanism as for compound semiconductors. In the present calculation the experimental NDM is reasonably well reproduced. Both upper valleys and nonparabolicity of the lower valleys are included in the model and the contributions of these two features can be separately evaluated. Figure 8 shows theoretical results for the drift-velocity at 77 K obtained with different models. It can be seen from there that in our model both nonparabolicity and electron transfer to upper valleys give an effective contribution to the NDM phenomenon.

Anisotropy of the drift velocity with respect to the direction of the applied field is present both in experimental and theoretical results. As is well known[37] this effect is due to a valley repopulation which is present when $\vec{E}$ is parallel to a ⟨111⟩ direction. The anisotropy decreases as T increases since intervalley scattering tends to equalize the mean energies of the electrons in cold and hot valleys. For $T = 240$ K, in fact, the anisotropy in our experimental results is of the same order as the experimental uncertainty of the data ($\pm 5\%$) and it has not been reported. At lower temperatures the theoretical anisotropy appears to be too small at very high fields.

With further research on the best fitting parameters in the theoretical model the overall agreement can be probably improved.

At the lowest temperatures ($T \leq 20$ K) the theoretical curve for $\vec{E} \parallel \langle 111 \rangle$ is interrupted toward the low fields. This is due to the difficulty of simulating the correct valley repopulation when intervalley scattering is very rare, as is reported for silicon in Ref. 1.

Section II D reports that the experimental electron drift velocity at these values of field and temperature is also strongly influenced by electron-electron interaction. This mechanism, in fact, tends to transfer energy from hot to cold valleys through e-e collisions, thus reducing the valley repopulation and therefore the drift velocity anisotropy.

Theoretical calculations have been performed[18] which include e-e interaction. A change in the aniso-

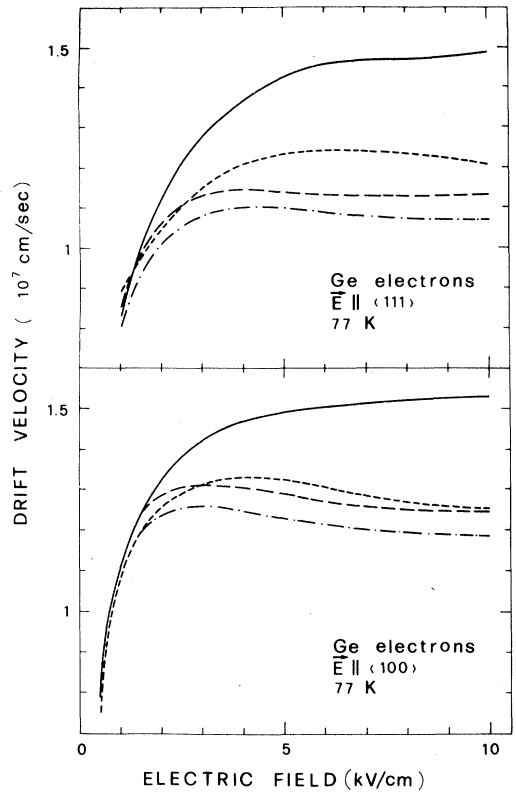

FIG. 8. Theoretical results for the electron drift velocity at 77 K for the electric field applied parallel to ⟨111⟩ and ⟨100⟩ crystallographic directions. The data are obtained with different models: —— parabolic valleys without upper valleys; --- nonparabolic valleys without upper valleys; – – – – – – parabolic valleys with upper valleys; and —·— nonparabolic valleys with upper valleys.

tropy of the drift velocity has been seen in the right direction in these cases, but is not sufficient to account for the experimental findings. The theoretical treatments, however, are not immune from possible criticisms, and the statistical uncertainty on the data given in Ref. 18 is rather high; before invoking other physical phenomena a better theoretical analysis of the e-e effect should be done.

Let us recall that with respect to other experimental results on this phenomena, the present data have the advantage of being obtained by varying the electron concentration in single samples without changing, therefore, the impurity concentration.

C. Diffusion

The diffusion properties of electrons in germanium along the electric field have been discussed in a previous publication[8]; for completeness we report here only the major conclusions.

The longitudinal diffusion coefficients as functions of the applied field are shown, in Fig. 5, for two temperatures; theoretical Monte Carlo results are here compared with experimental data. A very strong anisotropy of D_l can be seen, due to intervalley diffusion[8] when $\vec{E}$ is applied along a ⟨111⟩ direction. In this case, in fact, the different drift velocities of electrons in different valleys give rise to an additional spreading of the carriers besides the normal "thermal" diffusion.

For comparison some theoretical results obtained with the germanium model proposed in Ref. 4 are also shown in Fig. 5, which feature a too large intervalley diffusion. This comparison suggested a change in the intervalley coupling constant with respect to that model.

D. Valley repopulation

Figure 9 shows the populations of the different valleys as functions of the electric field applied along a ⟨111⟩ direction at three different temperatures. It can be seen that the population N_h of the hot valleys first decreases and then, after a minimum (which is about zero at 8 K), increases again toward its equilibrium value 0.75, since intervalley scattering tends to equalize the mean energy in all valleys. However, when electrons begin to populate the upper valleys N_h decreases again so that a wavy behavior is obtained. Similar and opposite considerations hold for the population N_c of the cold valleys.

The total effect is reduced as the temperature increases for the well-known reasons recalled in discussing the anisotropy of the drift velocity.

In Fig. 9 together with theoretical results, experimental results are shown obtained with the scaling technique[38,39] from the experimental drift velocity results shown in Figs. 1–3. This technique allows the determination of N_h and N_c only in the region of fields in which the upper valleys are not populated.

The agreement between experimental and theoretical results is very good at 8 and 20 K; however the range of the experimental data does not cover the field of maximum repopulation at these lower temperatures. At 45 K the discrepancy in the position of the maximum anisotropy of the drift velocity (see Fig. 3) shows up clearly in the repopulation curves.

E. Electron distribution function

Figure 10 shows the distribution of electrons in the lower valleys as obtained from the Monte Carlo calculations as a function of energy at 77 K for different values of the electric field applied along a ⟨100⟩ direction. The main features are the same as shown in Ref. 4 and for this reason we do not report these distributions for other field directions or other valleys. At intermediate fields the distribution shows the kinks around the energy of intervalley and optical

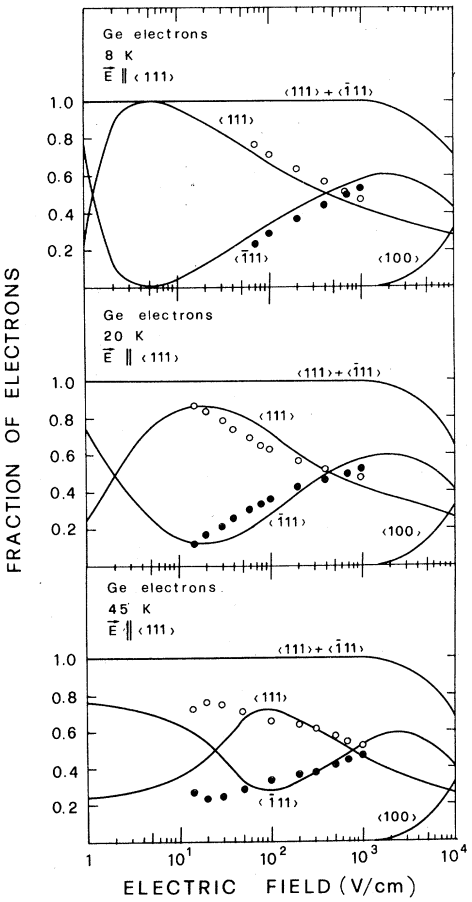

FIG. 9. Electron populations of the different valleys as functions of electric field applied along a ⟨111⟩ direction at three different temperatures. Continuous lines indicate the theoretical results obtained with the Monte Carlo simulation. Closed and open circles indicate experimental results for the hot- and cold-valley populations, respectively, obtained with the scaling technique from the experimental drift velocity data shown in Figs. 1–3.

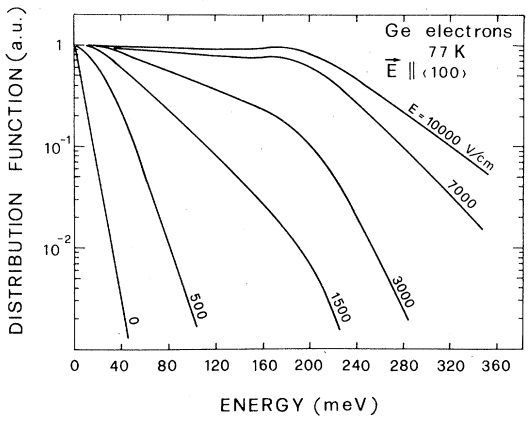

FIG. 10. Electron distribution in the lower valleys as obtained from the Monte Carlo calculations as a function of energy at 77 K for different values of the electric fields applied along a ⟨100⟩ crystallographic direction.

phonons and at the energy of the bottom of the upper valleys while at the highest field strengths only the latter remain.

F. Electron mean energy

The electron mean energy in the lower valleys as a function of the electric field applied along a ⟨100⟩ direction is shown in Fig. 11 for different lattice temperatures.

For fields oriented along a ⟨111⟩ direction, a difference between hot and cold valleys is obviously found. The effect is similar to that reported for electrons in Si[1] and will not be reported here.

More interesting is the comparison of the electron mean energy for $\vec{E} \parallel \langle 100 \rangle$ in the four models discussed in Sec. IV B above: (a) parabolic valleys

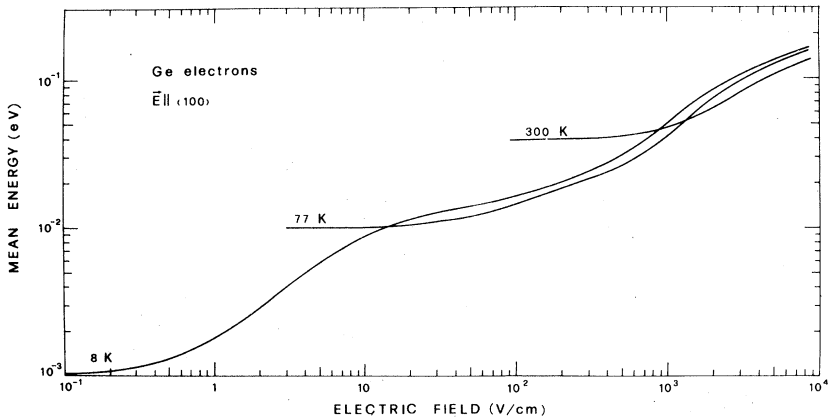

FIG. 11. Electron mean energy in the lower valleys as a function of electric field applied along a ⟨100⟩ direction for three different lattice temperatures. Data have been obtained from Monte Carlo calculations.

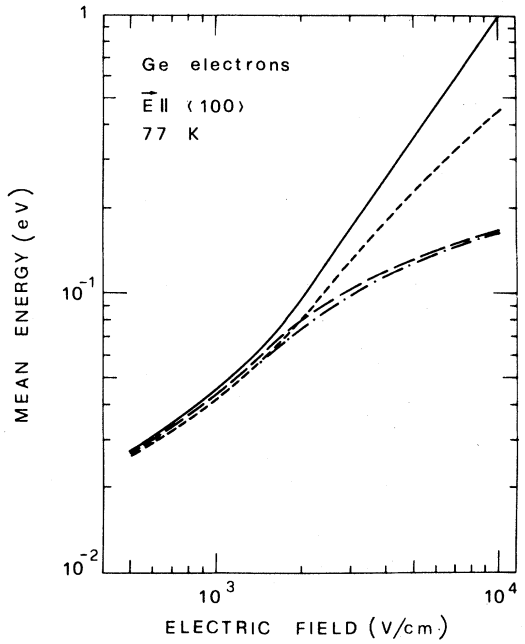

FIG. 12. Theoretical electron mean energy for $\vec{E} \parallel \langle 100 \rangle$ at 77 K obtained with the four models discussed in Sec. IV B of the text: —— parabolic valleys without upper valleys; —— —— parabolic valleys with upper valleys; — — — nonparabolic valleys without upper valleys, and —·—· nonparabolic valleys with upper valleys.

without upper valleys; (b) nonparabolic valleys without upper valleys; (c) parabolic valleys with upper valleys; and (d) nonparabolic valleys with upper valleys.

This comparison is shown in Fig. 12 for $T = 77$ K and it may be seen that the effect of nonparabolicity is strong if upper valleys are neglected, but when they are considered nonparabolicity is much less effective.[4]

G. Energy relaxation time

Figure 13 shows for several temperatures the theoretical electron energy relaxation time, defined by [40,41]

$$\tau_\epsilon = \frac{\langle \epsilon(E) \rangle - \epsilon_0}{e v_d E} , \tag{3}$$

where e is the electron charge, $\langle \epsilon(E) \rangle$ the average electron energy as a function of field strength applied parallel to a ⟨100⟩ direction. In evaluating τ_ϵ from Eq. (3), $\langle \epsilon \rangle$ and v_d have been taken from the Monte Carlo calculations.

The theoretical curve for $T = 77$ K is compared in Fig. 14 with the experimental results of Dargys and Banys[42] who obtained τ_ϵ from second harmonic generation measurements. The agreement is very good in this case. The sharp initial fall is due to the increasing efficiency of optical and intervalley scattering as the electrons are heated by the field. This interpretation is confirmed by considering the energy dissipation rates due to the different scattering mechanisms which are discussed in the next section.

H. Energy and velocity dissipation rates

In Fig. 15 the energy and momentum dissipation rates for all scattering mechanisms considered in the lower valleys are shown as a function of field strength applied parallel to a ⟨100⟩ direction at $T = 77$ K.

It may be seen that at this temperature acoustic scattering is dominant at low fields for momentum dissipation but negligible for energy dissipation. This last is essentially due, at low field, to optical and equivalent intervalley scattering. At highest fields nonequivalent intervalley scattering is the most im-

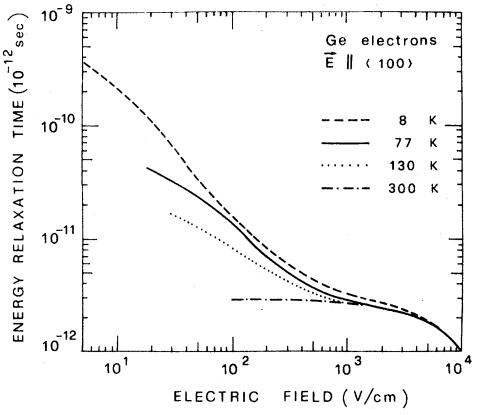

FIG. 13. Theoretical electron energy relaxation time (see text) as a function of electric field applied parallel to a ⟨100⟩ crystallographic direction at four temperatures.

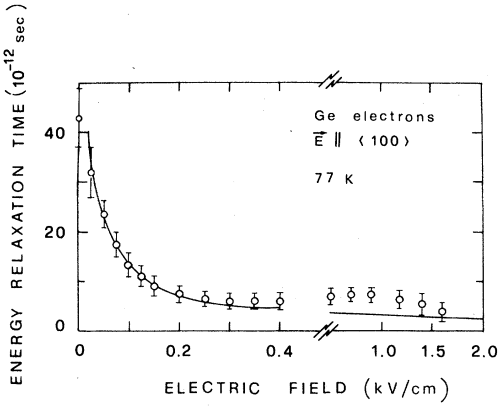

FIG. 14. Comparsion between present theoretical electron energy relaxation time and experimental results of Dargys and Banys in Ref. 42 at 77 K and for electric fields applied along a ⟨100⟩ crystallographic direction.

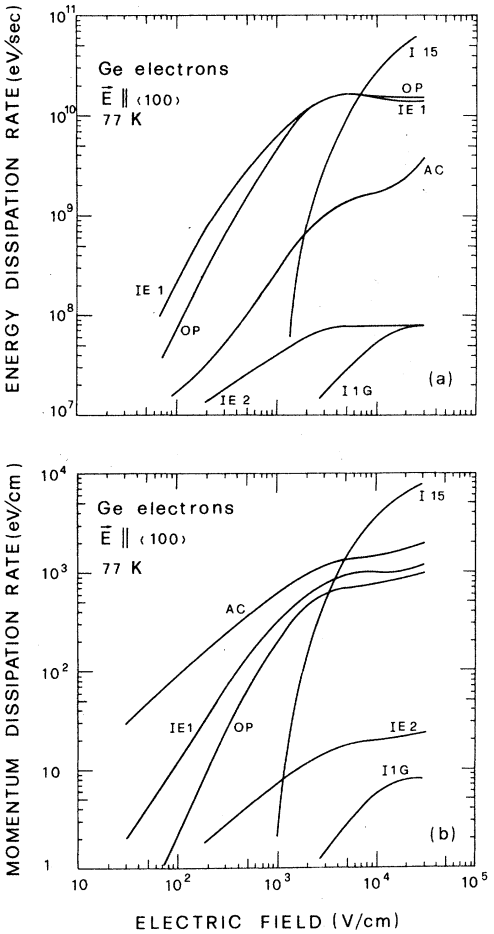

FIG. 15. Monte Carlo results for the energy (a) and momentum (b) dissipation rates due to the various scattering mechanisms in the lower valleys as functions of field applied along a ⟨100⟩ direction at 77 K. The symbols are those listed in Table I.

portant one in dissipating both energy and momentum.

The dissipation rates refer to the total simulation time, so that they already include the reduction of efficiency due to valley depopulation at high fields.

V. CONCLUSIONS

In this paper an extensive investigation, both experimental and theoretical, on electron transport properties in Ge has been presented. In particular, the drift velocity of electrons has been measured with the time-of-flight technique in wide range of temperatures and electric fields.

The technique, especially suitable for high-resistivity material, enabled us to perform the measurements on hyperpure samples.

Longitudinal diffusion measurements have also been included in order to give a more complete picture of electron transport in Ge.

The theoretical interpretation of the experimental results has been performed with the Monte Carlo technique. The model includes lower, ⟨111⟩, nonparabolic bands as well as upper bands at the center of the Brillouin zone along the ⟨100⟩ directions. Acoustic scattering has been considered with proper energy relaxation also in the nonparabolic valleys. In addition, optical scattering has been taken into account in the lowest valleys together with intervalley scattering between nonequivalent valleys.

The NDM effect at the lowest temperatures for fields along ⟨100⟩ directions is found to be due to both upper valleys and to nonparabolicity of the lower valleys with a larger contribution of the former cause.

In certain cases the theoretical predictions have been compared also with experiment data, other than the present ones, available in the literature.

Besides the results to be compared with experimental data, other quantities such as the mean electron energy, the dissipation rates of energy and velocity by the various scattering mechanisms, the electron distribution function and the valley repopulation, have been worked out from the Monte Carlo simulation, in order to get a complete physical picture of the electron transport process in Ge.

ACKNOWLEDGMENTS

The authors wish to thank Dr. L. Reggiani for valuable comments and suggestions and are grateful to Professor A. Alberigi Quaranta for constant interest and support. Computer facilities were kindly provided by the Computer Center of Modena University. This work has been partially supported by Consiglio Nazionale delle Ricerche, Italy.

APPENDIX

In this appendix we shall describe how intravalley acoustic scattering has been treated in our Monte Carlo calculation. In particular, the simultaneous consideration of the nonparabolicity of the valleys and of the correct acoustic energy dissipation is the novel element of the calculation.

A squared matrix element of the form

$$|H'|^2=\frac{E_1^2\hbar q}{2V\rho v_s}\begin{Bmatrix} N_q \\ N_q+1 \end{Bmatrix} \tag{A1}$$

has been assumed, where E_1, is the deformation-potential constant, V and ρ are the volume and the density of the crystal, v_s is the velocity of sound, and

q and N_q are the phonon wave vector and distribution, respectively; N_q or N_q+1 must be taken for absorption or emission, respectively. By application of the golden rule the matrix element in Eq. (A1) yields the scattering rate

$$P_{ac}d^3q = \frac{E_1^2 q}{8\pi\rho v_s}\begin{pmatrix} N_q \\ N_q+1 \end{pmatrix} \times \delta(\epsilon(\vec{k}\pm\vec{q})-\epsilon(\vec{k})\pm\hbar q v_s)d^3q \quad , \quad \text{(A2)}$$

where the upper or lower sign must be taken for absorption or emission, respectively.

Transforming to the starred space with the Herring and Vogt transformation[19] we make the spherical approximation

$$q = q^*\left[\frac{m_l}{m_0}\cos^2\theta^* + \frac{m_t}{m_0}\sin^2\theta^*\right]^{1/2} \approx q^*\left[\frac{m_D}{m_0}\right]^{1/2} , \quad \text{(A3)}$$

where θ^* is the angle between $\vec{q}^*$ and the principal axis of the valley, m_0 the free-electron mass, and m_D the density-of-states effective mass $(m_l m_t^2)^{1/3}$.

Taking into account the energy–wave-vector relationship given in Eq. (2), the requirement for a vanishing argument of the δ of energy conservation yields

$$\cos\theta = \pm\frac{q^*}{2k^*}(1-4\alpha\epsilon_s^*) + \left[\frac{\epsilon_s^*}{\gamma}\right]^{1/2}(1+2\alpha\epsilon) \quad , \quad \text{(A4)}$$

where θ is the angle between $\vec{q}^*$ and $\vec{k}^*$ and

$$\epsilon_s^* = \tfrac{1}{2}m_D v_s^2 \quad . \quad \text{(A5)}$$

As in the standard procedure,[37] the condition of $|\cos\theta| \leq 1$ yields the limit of variability of q^*. For our purposes it is more convenient to express these limits

TABLE II. Limits of integration of the variable $x = \hbar q v_s/(kT)$ for acoustic scattering.

Absorption	$x_1 = C^*(\alpha)[(\epsilon_s^*)^{1/2}(1+2\alpha\epsilon) - \sqrt{\gamma}]$ $\kappa_2 = C^*(\alpha)[(\epsilon_s^*)^{1/2}(1+2\alpha\epsilon) + \sqrt{\gamma}]$
$\gamma \leq \gamma_s$ No emission	
Absorption	$x_1 = 0$ $x_2 = C^*(\alpha)[\sqrt{\gamma} + (\epsilon_s^*)^{1/2}(1+2\alpha\epsilon)]$
$\gamma > \gamma_s$ Emission	$x_1 = 0$ $x_2 = C^*(\alpha)[\sqrt{\gamma} - (\epsilon_s^*)^{1/2}(1+2\alpha\epsilon)]$

$$C^*(\alpha) \equiv \frac{6(\epsilon_s^*)^{1/2}}{kT(1-4\alpha\epsilon_s^*)} \qquad \gamma_s = \frac{\epsilon_s^*}{1-4\alpha\epsilon_s^*}$$

for the dimensionalless variable

$$x \equiv \frac{\hbar q v_s}{kT} = \frac{\hbar q^* v_s}{kT}\left[\frac{m_D}{m_0}\right]^{1/2} . \quad \text{(A6)}$$

These limits are given in Table II under the condition, verified in our case, that $4\alpha\epsilon_s^* < 1$. The transition rate is then given by

$$P_{ac}dx = \frac{A_a}{\sqrt{\gamma}}\begin{pmatrix} N_q(x) \\ N_q(x)+1 \end{pmatrix}(1+2\alpha\epsilon \pm 2\alpha kTx)x^2dx \quad , \quad \text{(A7)}$$

where

$$A_a \equiv \left[\frac{E_1 m_D}{4\hbar^2}\right]^2 \frac{1}{\pi\rho v_s}\frac{(kT)^3}{\epsilon_s^{*3/2}} \quad . \quad \text{(A8)}$$

For $N_q(x)$ a very good approximation is necessary in order to have a correct description of energy balance at low temperatures.[1] We found it convenient to use different approximations for $N_q(x)$ and for $N_q(x)+1$:

$$N_q(x) = \begin{cases} \dfrac{1}{x} - \tfrac{1}{2} + \tfrac{1}{12}x - \dfrac{x^3}{720} + \dfrac{x^5}{30\,240} - \dfrac{x^7}{1\,209\,600} + \dfrac{x^9}{47\,900\,160}, & x \leq 3.5 \\ e^{-x}, \quad x > 3.5 \quad , \end{cases} \quad \text{(A9)}$$

$$N_q(x)+1 = \begin{cases} \dfrac{1}{x} + \tfrac{1}{2} + \tfrac{1}{12}x - \dfrac{x^3}{720} + \dfrac{x^5}{30\,240}, & x < 4 \quad , \\ 1, \quad x \geq 4 \quad . \end{cases} \quad \text{(A10)}$$

The integration of the scattering rate in Eq. (A7) can then be performed very easily. To determine the state of the scattering, the expression of $P_{ac}dx$ in Eq. (A7) has been used to select with the aid of the rejection technique.[20] The state after scattering is then determined by simple geometrical considerations of energy and momentum conservation. The angle of rotation around the initial state is random.

[1]C. Canali, C. Jacoboni, F. Nava, G. Ottaviani, and A. Alberigi Quaranta, Phys. Rev. B 12, 2265 (1975).
[2]G. Ottaviani, L. Reggiani, C. Canali, F. Nava, and A. Alberigi Quaranta, Phys. Rev. B 12, 3318 (1975).
[3]L. Reggiani, C. Canali, F. Nava, and G. Ottaviani, Phys. Rev. B 16, 2781 (1977).
[4]W. Fawcett and E. G. S. Paige, J. Phys. C 4, 1801 (1971).
[5]W. P. Dumke, Phys. Rev. B 2, 987 (1970).
[6]W. E. Spear, J. Non-Cryst. Solids 1, 197 (1968).
[7]G. Ruch and G. Kino, Phys. Rev. 174, 174 (1968).
[8]C. Canali, C. Jacoboni, and F. Nava, Solid State Commun. 26, 889 (1978).
[9]F. Nava, C. Canali, F. Catellani, G. Gavioli, and G. Ottaviani, J. Phys. C 9, 1685 (1976).
[10]J. W. Sigmon and J. F. Gibbons, Appl. Phys. Lett. 15, 320 (1969).
[11]F. Nava, C. Canali, and C. Jacoboni, Solid State Electron. 21, 689 (1978).
[12]L. Reggiani, C. Canali, F. Nava, and A. Alberigi Quaranta, J. Appl. Phys. 49, 4446 (1978).
[13]G. Ottaviani, V. Marello, J. W. Mayer, N-A. Nicolet, and J. M. Caywood, Appl. Phys. Lett. 20, 323 (1972).
[14]J. E. Smith, Jr., Phys. Rev. 178, 1364 (1969).
[15]C. Canali, C. Jacoboni, G. Ottaviani, and A. Alberigi Quaranta, Appl. Phys. Lett. 27, 278 (1975).
[16]M. Asche, B. L. Boichenko, V. M. Bondar, and G. O. Sarbei, Phys. Status Solidi B 44, 173 (1971).
[17]J. G. Nash and J. W. Holm-Kennedy, Appl. Phys. Lett. 24, 139 (1975).
[18]C. Jacoboni, in *Proceedings of the 13th International Conference on the Physics of Semiconductors, Rome, 1976,* edited by F. G. Fumi (North-Holland, Amsterdam, 1977), p. 1195.
[19]C. Herring and E. Vogt, Phys. Rev. 101, 944 (1955).
[20]W. Fawcett, D. A. Boardman, and S. Swain, J. Phys. Chem. Solids 31, 1963 (1970).
[21]A. Alberigi Quaranta, C. Jacoboni, and G. Ottaviani, Rivista Nuovo Cimento. 1, 445 (1971).
[22]W. Fawcett and H. D. Rees, Phys. Lett. A 29, 587 (1969).
[23]V. Borsari and C. Jacoboni, Phys. Status Solidi B 54, 649 (1972).
[24]E. G. S. Paige, in *Progress in Semiconductors,* edited by A. F. Gibson and R. E. Burgers (Heywood, London, 1964), Vol. 8.
[25]M. L. Cohen and T. K. Bergstresser, Phys. Rev. 141, 789 (1966).
[26]D. J. Stukel, Phys. Rev. B 3, 3347 (1971).
[27]F. J. Morin, Phys. Rev. 93, 62 (1954).
[28]E. M. Conwell and P. P. Debye, Phys. Rev. 93, 693 (1954).
[29]M. B. Prince, Phys. Rev. 130, 2201 (1953).
[30]R. D. Brown, S. H. Koening, and W. Schillinger, Phys. Rev. 128, 1688 (1962).
[31]R. S. de Biasi and S. S. Yee, J. Appl. Phys. 43, 609 (1972).
[32]A. S. Baynham, IBM J. Res. Dev. 13, 568 (1969).
[33]M. I. Nathan, Phys. Rev. 130, 2201 (1963).
[34]D. M. Chang and J. Ruch, Appl. Phys. Lett. 12, 111 (1968).
[35]G. S. Kino and A. Neukermans, Phys. Rev. 7, 2693 (1973).
[36]J. B. Elliot, J. B. Gunn, and J. C. McGroddy, Appl. Phys. Lett. 11, 253 (1967).
[37]E. M. Conwell, in *High Field Transport in Semiconductors, Solid State Phys. Suppl.* (Academic, New York, 1967), Vol. 9.
[38]D. Schweitzer and K. Seeger, Z. Phys. 183, 207 (1965).
[39]J. W. Holm-Kennedy and K. S. Champlin, Appl. Phys. Lett. 16, 46 (1970).
[40]A. F. Gibson, J. W. Granville, and E. Paige, in *Proceedings of the 5th International Conference on the Physics of Semiconductors, Prague, 1960* (Academic, New York, 1960), p. 112; J. Phys. Chem. Solids 19, 198 (1961).
[41]T. N. Morgan and C. E. Kelly, Phys. Rev. 137, A1537 (1965).
[42]A. Dargys and T. Banys, Phys. Status Solidi B 52, 699 (1972).